



HAL
open science

Spin State Chemistry: Modulation of Ligand pKa by Spin State Switching in a [2'2] Iron(II) Grid-Type Complex

Sébastien Dhers, Abhishake Mondal, David Aguilà, Juan Morua Ramirez, Sergi Vela, Pierre Dechambenoit, Mathieu Rouzieres, Jonathan R Nitschke, Rodolphe Clérac, Jean-Marie Lehn

► **To cite this version:**

Sébastien Dhers, Abhishake Mondal, David Aguilà, Juan Morua Ramirez, Sergi Vela, et al.. Spin State Chemistry: Modulation of Ligand pKa by Spin State Switching in a [2'2] Iron(II) Grid-Type Complex . Journal of the American Chemical Society, 2018, 140 (26), pp.8218 - 8227. 10.1021/jacs.8b03735 . hal-01848265

HAL Id: hal-01848265

<https://hal.science/hal-01848265v1>

Submitted on 24 Jul 2018

HAL is a multi-disciplinary open access archive for the deposit and dissemination of scientific research documents, whether they are published or not. The documents may come from teaching and research institutions in France or abroad, or from public or private research centers.

L'archive ouverte pluridisciplinaire **HAL**, est destinée au dépôt et à la diffusion de documents scientifiques de niveau recherche, publiés ou non, émanant des établissements d'enseignement et de recherche français ou étrangers, des laboratoires publics ou privés.

Spin State Chemistry: Modulation of Ligand pKa by Spin State Switching in a [2×2] Iron(II) Grid-Type Complex

Sébastien Dhers,[†] Abhishake Mondal,^{‡,§} David Aguilà,^{‡,#} Juan Ramírez,[†] Sergi Vela,[◇] Pierre Dechambenoit,^{‡,#} Mathieu Rouzières,^{‡,#} Jonathan R. Nitschke,^{†,⊥} Rodolphe Clérac,^{*,‡,#} and Jean-Marie Lehn^{*,†}

[†] Laboratoire de Chimie Supramoléculaire, ISIS, Université de Strasbourg, 8 Allée Gaspard Monge, 67000 Strasbourg, France


[‡] CNRS, CRPP, UMR5031, F-33600 Pessac, France

[#] Univ. Bordeaux, CRPP, UMR5031, F-33600 Pessac, France

[§] Solid State and Structural Chemistry Unit, Indian Institute of Science, C.V. Raman Road, Bangalore-560012, India

[◇] Laboratoire de Chimie Quantique, UMR 7177 CNRS-Université de Strasbourg, 1 rue Blaise Pascal, 67008 Strasbourg, France

[⊥] Department of Chemistry, University of Cambridge, CB2 1EW, UK

 Supporting Information

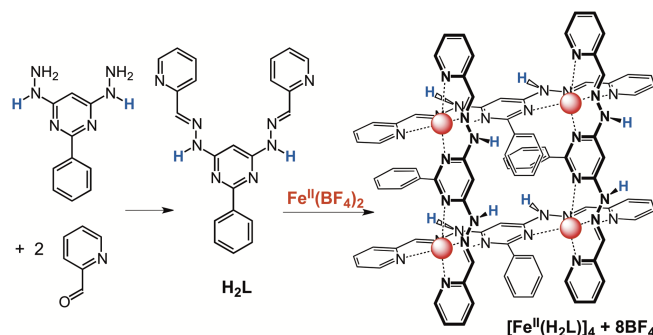
ABSTRACT: The iron(II) [2×2] grid complex **Fe-8H** has been synthesized and characterized. It undergoes spin-crossover (SCO) upon deprotonation of the hydrazine-based terpyridine-like ligand. The deprotonation patterns have been determined by X-ray crystallography and ¹H NMR spectroscopy and discussed in relation to the spin state of the iron(II) centers which influences greatly the pKa of the ligand. The synthesis of the magnetically-silent zinc(II) analogue is also reported and its (de)protonation behavior has been characterized to serve as reference for the study of the Fe^{II} grid complexes. DFT computations have also been performed in order to investigate how the successive deprotonation of the bridging ligands affects the SCO behavior within the grid.

■ INTRODUCTION

The search for materials having tunable properties is a very active research area.¹ In this context, special attention has been given to the modulation of magnetic properties by physical means such as temperature,² pressure and light,^{2,3} or through chemical processes affecting the ligand field in complexes.⁴ Spin crossover (SCO) complexes are interesting candidates, particularly iron(II) complexes, which exhibit a switching process between a paramagnetic high spin state (HS, $S = 2$) and a diamagnetic low spin state (LS, $S = 0$).⁵ Polymetallic [2×2] grid-like complexes⁶ with modulable properties can be seen as molecular precursors of metallosupramolecular architectures or materials due to their ability to generate ordered arrangements of multiple grid entities by self-assembly at the air-water interface,⁷ through hydrogen-bond formation in the solid array⁸ and on adsorption onto a graphite surface.⁹ It has been shown that tetranuclear iron(II) [2×2] grids undergo multiple spin state switching under the action of three physical triggers, temperature, pressure and light.^{2,10} The influence of hydrogen-bond donors,¹¹ as well as that of counterions and solvent,¹² have also been shown to allow the modulation of the magnetism of these architectures. On the other hand, [2×2] grids presenting ionizable N-H sites undergo reversible protonic modulation of optical and redox properties.¹³ One thus expects that the magnetic properties of such entities may also be modulated by reversible ligand deprotonation without destruction of the initial complex.^{2,13} The hydrazine-based ditopic isomeric ligand **H₂L** (Scheme 1) offers the opportunity to both generate [2×2] grid architectures by self-assembly and to study the protonic modulation of their physico-chemical properties, due to their ionizable N-H sites. The final step of the synthesis of such a ditopic ligand consists in the condensation reaction of one equivalent of

4,6-bis(hydrazino)-2-phenyl-pyrimidine with two equivalents of 2-pyridine-carboxaldehyde to yield ligand **H₂L**. This ligand contains two complexation subunits of terpyridine (**terpy**) type, where the hydrazone function acts as an ionizable group whose acidity is greatly enhanced on complexation, as compared to the free ligands.

Scheme 1. Synthesis of the ditopic ionizable hydrazine-based ligand **H₂L and its self-assembly into the corresponding tetranuclear [Fe₄(H₂L)₄]⁸⁺ [2×2] grid complex by coordination with Fe^{II} cations. Red spheres represent Fe metal ions. Hydrogen atoms that are colored in blue emphasize the deprotonation sites on the [2×2] grid.**



The iron(II) $[2 \times 2]$ grid $[\text{Fe}_4(\text{H}_2\text{L})_4]^{8+}$ shown in Scheme 1 incorporates hydrazone groups, which act as soft ligands to assemble the iron(II) ions. The deprotonation of this two-site ligand H_2L ¹⁴ changes its coordination properties from a weak-field ligand (non-deprotonated) to a strong-field ligand (deprotonated). Its deprotonation also confers to the ligand an anionic¹⁵ character ($-\text{N}=\text{N}=\text{CH}^-$, Scheme S1) thus leading to a stronger coordination with a larger splitting energy between the e_g and t_{2g} levels of the iron cations. In this configuration, all the electrons should be paired in the t_{2g} level leading to a diamagnetic $[\text{Fe}_4\text{L}_4]$ complex. However, given that a grid complex contains four Fe^{II} cations, the spin cross-over process may be more or less complete depending on the strength of the ligand field. This modulation of the magnetic properties is expected to depend on the degree of deprotonation of the grid, which contains a total of eight ionizable groups. Indeed, the influence of pH on iron(II) SCO complexes has been investigated mostly in the context of NMR contrast agents¹⁶ and only a few pH switchable iron(II) SCO complexes have been reported just for single iron(II) sites.¹⁷

Herein, we describe the synthesis of the iron(II) $[2 \times 2]$ grid complex, $[\text{Fe}_4(\text{H}_2\text{L})_4]^{8+}$, and the study of the reversible modulation of its magnetic properties in the solid state and solutions depending on the protonation state of the four constituting ligands. We also demonstrate the remarkable effect of the iron(II) spin state switching on the pKa of the grid ligands, which induces the generation of selectively deprotonated magnetic entities and amounts conversely to a spin state modulated chemical reaction. The zinc(II) analogue is also reported and serves as a diamagnetic reference compound for the investigation of the iron(II) grid entities.

RESULTS AND DISCUSSION

Synthesis of the ligand and of the corresponding Fe^{II} $[2 \times 2]$ grid complexes. Several $[2 \times 2]$ grids, $[\text{Fe}_4(\text{H}_n\text{L}_4)]^{(n)+}$ ($0 > n > 8$, $\text{Fe}-n\text{H}$), were prepared and isolated by reaction of the corresponding ligand H_2L with $\text{Fe}(\text{BF}_4)_2$ in a 1:1 molar ratio at room temperature in acetonitrile and in the case of $n < 8$, adding the corresponding amount of base (triethylamine) for deprotonation (see supporting information for detailed procedures). Subsequently, crystals of the $[2 \times 2]$ grid complexes in different states of ionization were obtained by slow diffusion of diethyl-ether into the different solutions. Three single-crystal structures were determined by X-ray diffraction (see supporting information) and confirmed the expected $[2 \times 2]$ grid topology accompanied by 8, 6 and 4 BF_4^- anions, depending on the degree of deprotonation of the grids: $[\text{Fe}_4(\text{H}_2\text{L})_4](\text{BF}_4)_{8-x}\text{MeCN}$ (**Fe-8H**, red needles, $x = 2$ or 6 at 290 and 120 K, respectively), $[\text{Fe}_4(\text{H}_2\text{L})_2(\text{HL})_2](\text{BF}_4)_6\text{8MeCN}$ (**Fe-6H**, red blocks) and $[\text{Fe}_4(\text{HL})_4](\text{BF}_4)_4\text{12MeCN}$ (**Fe-4H**, red plates). Unfortunately, and despite intensive efforts, no crystals were obtained for the other deprotonated states. Two Zn-based $[2 \times 2]$ grids, $[\text{Zn}_4(\text{H}_n\text{L}_4)]^{(n)+}$ ($n = 8$ and 4, **Zn-8H** and **Zn-4H**, respectively), were also prepared and isolated by reaction of the corresponding ligand with $\text{Zn}(\text{BF}_4)_2$ in a 1:1 molar ratio at room temperature in acetonitrile (in the case of $n = 4$, the corresponding amount of triethylamine was added). As zinc(II) is diamagnetic, the Zn-based complexes provide model systems to study the ligand behavior independently of the iron(II) SCO influence.

Solid state molecular structures and spin states of the $[\text{Fe}_4(\text{H}_n\text{L}_4)]^{(n)+}$ ($n = 8, 6, 4$) and $[\text{Zn}_4(\text{HL})_4](\text{BF}_4)_4$ $[2 \times 2]$ grid complexes in different ionization states. (a) The red needle crystals of **Fe-8H** were found to lose crystallinity rapidly once outside the mother liquor. Thus, a single-crystal was mounted immersed in oil and placed in the X-ray diffractometer directly at 120 K. The crystal structure was solved in the monoclinic $C2/c$ space group, exhibiting a molecular $[2 \times 2]$ grid topology with the four fully protonated ligands: $[\text{Fe}_4(\text{H}_2\text{L})_4](\text{BF}_4)_8\text{6MeCN}$ (**Fe-8H**, Table S1, top part of Figure 1 and Figure S2). Together with the cationic complex, eight tetrafluoroborate

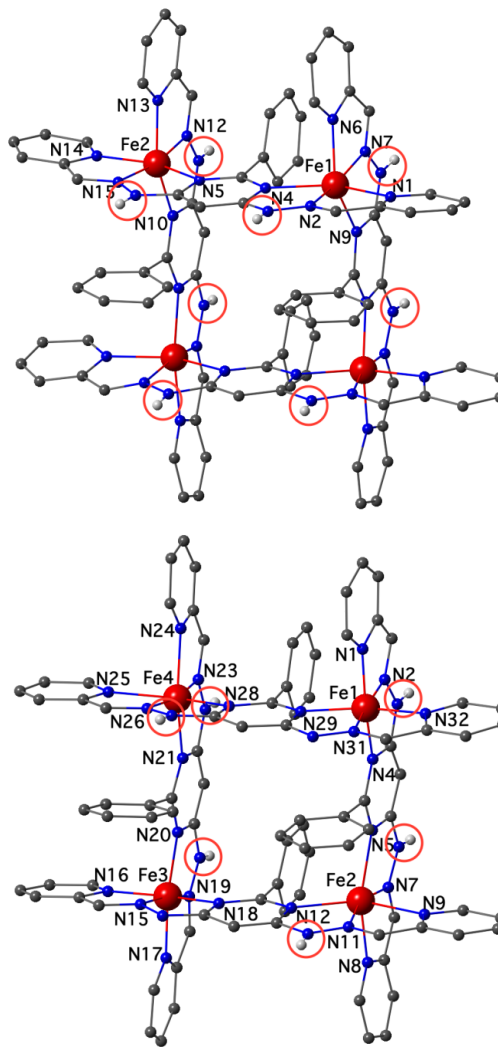


Figure 1. Ball and stick representations of the crystal structures of the $[\text{Fe}_4(\text{H}_2\text{L})_4](\text{BF}_4)_8 \cdot 2\text{MeCN}$ complex, **Fe-8H**, with non-ionized ligands (top) and the doubly deprotonated $[\text{Fe}_4(\text{H}_2\text{L})_2(\text{HL})_2](\text{BF}_4)_6 \cdot 8\text{MeCN}$ complex, **Fe-6H**, (bottom) both at 290 K. Fe, N, C and H atoms are shown in red, blue, grey and white, respectively. All non-NH hydrogen atoms, acetonitrile and tetrafluoroborate molecules are omitted for clarity. Non-deprotonated NH sites are circled in red.

anions ensure the electro-neutrality of the system and indicate the 8+ charge of the corresponding **Fe-8H** complex. In addition, acetonitrile molecules are located in the crystal lattice. The number of acetonitrile molecules (six) was derived from the electron density and void space volume calculated by PLATON. In the asymmetric unit, one of the BF_4^- anions is disordered across two positions, as is the phenyl group of one of the H_2L ligands. Two types of iron ions, Fe1 and Fe2, were found in the asymmetric unit, both exhibiting coordination number six. The bond distances between Fe1 and the corresponding nitrogen donor atoms (1.885(9) – 2.060(7) Å, Table S3) suggest a low spin configuration. In contrast, the Fe2-N bond distances are in the range between both low and high spin configurations (1.971(7) – 2.133(7) Å, Table S3) suggesting possible spin state disorder on this site. The H_2L ligands show hydrogen bonding interaction between their corresponding acidic NH protons and (i) two BF_4^- anions around the Fe2 site and (ii) one BF_4^- anion and one acetonitrile molecule around the Fe1 centers.

The temperature of the same single crystal was then increased at 2 K min^{-1} up to 290 K. The collected structure was again solved in the

monoclinic $C2/c$ space group, with the same $[2 \times 2]$ -grid like geometry (Table S1). The complex is thus surrounded by the eight tetrafluoroborate anions, two of them being disordered. The number of acetonitrile molecules has been estimated to be two. Thus, the increase of temperature to 290 K seems to favor the loss of about four acetonitrile molecules. This desolvation effect is clearly seen in the reduction of the unit cell volume, which contracts from 11904.6(17) Å³ at 120 K to 11151(3) Å³ at 290 K (Table S1). The Fe2 site and its coordination sphere appears to be only slightly affected by the temperature change with Fe2-N bond distances ranging between 1.980(8) and 2.127(8) Å (Table 1 and Table S3). As observed at 120 K, the spin state of the Fe2 ion is thus in between LS and HS, in agreement with a possible spin state disorder on this site. On the other hand, the bond distances between the Fe1 site and the nitrogen donor atoms are much larger than at 120 K ranging between 2.081(8) and 2.196(8) Å. This modification of the Fe1 coordination site indicates clearly a spin-state switching from LS at 120 K to HS at 290 K and reveals the occurrence of a spin-crossover process in **Fe-8H**.

Table 1. Summary of the Fe^{II} spin states as deduced from the crystallographic data at 120 and 290 K for Fe-8H, Fe-6H, and Fe-4H.

	Fe-8H		Fe-6H		Fe-4H
	(red needles)		(red blocks)		(red plates)
	120 K	290 K	120 K	290 K	120 K
Fe1	LS	HS	LS	LS	LS
Fe2	LS-HS	LS-HS	LS-HS	HS	LS-HS
Fe3	LS	HS	LS	LS	LS
Fe4	LS-HS	LS-HS	LS-HS	HS	LS-HS

Note: the Fe3 and Fe4 sites are symmetry-equivalent to Fe1 and Fe2 in **Fe-8H**.

(b) Following the same procedure, a **red block** crystal of **Fe-6H** was mounted immersed in oil and placed in the X-ray diffractometer directly at 120 K. The crystal structure was collected and solved in the monoclinic $P2_1/c$ space group (Table S1), exhibiting again a $[2 \times 2]$ grid-like complex. However, in this case, only six tetrafluoroborate anions were found in the structure, since two ligands exhibit a monodeprotonation giving the complex: $[\text{Fe}_4(\text{HL})_2(\text{HL})_2](\text{BF}_4)_6 \cdot 8\text{MeCN}$ (**Fe-6H**, bottom part of Figure 1 and Figure S3). Together with the anions, eight molecules of acetonitrile are located in the crystal lattice. At this temperature, three pyridyl moieties are significantly disordered. Similarly, one of the acetonitrile molecules is disordered across three different positions, while one of the BF_4^- anions shows disorder between two different positions. Each of the six acidic NH protons is interacting with a molecule of tetrafluoroborate anion, while no H-bond acceptor is located close to the two deprotonated hydrazone groups. The $[2 \times 2]$ grid-like complex shows four crystallographically different iron sites (Figure 1, bottom). Fe1 and Fe3 are surrounded by two coordination pockets featuring one protonated and one deprotonated hydrazone group. The bond distances between the metal ion (Fe1 and Fe3) and the donor N atoms are in the range for a low spin configuration (1.875(3) – 2.035(3) Å for Fe1, 1.872(4) – 2.063 Å for Fe3, Table S4). In contrast, the coordination pockets around the Fe2 and Fe4 site feature two NH groups. The Fe2-N and Fe4-N bond distances do not point strongly toward a specific electronic configuration (2.010 – 2.165 Å and 1.904(6) – 2.113(4) Å, respectively; Table S4), although this feature could be influenced by the disorder exhibited by the pyridyl groups surrounding these two metal ions. The same single-crystal was allowed to warm to 290 K (2 K min⁻¹), and the structure was again collected (Table S1). While the same space group was used to solve the structure ($P2_1/c$), the volume of the unit cell was found to be significantly larger (11437.0(8) and 11889.2(18) Å³ at 120 and 290 K, respectively). At this temperature, only one tetrafluoroborate anion was found to be disordered. The Fe-N

bond distances around the two iron sites, Fe1 and Fe3, encapsulated by the coordination pocket featuring both protonated and deprotonated hydrazone group are very similar to the ones observed at 120 K, suggesting again a low spin configuration (1.871(4) – 2.043(4) Å and 1.871(4) – 2.053(4) Å for Fe1 and Fe3, respectively, Table S4). Thus, as expected, the deprotonation of the hydrazone group leads to a stronger ligand field and thus stabilizes the LS state of the coordinated iron metal ion. In contrast, the Fe-N bond distances around the Fe2 and Fe4 sites (surrounded by pockets featuring two non-deprotonated =N-NH- hydrazone groups) are now clearly in the range for a high-spin configuration (2.118(4) – 2.247(4) Å and 2.088(4) – 2.244(4) Å for Fe2 and Fe4, respectively, Table 1 and Table S4), evidencing a stabilization of the HS state at higher temperatures and suggesting the occurrence of a spin-crossover phenomena at these metal ion sites.

(c) The crystals of the third type, the **red plates**, were also collected at 120 K and solved in the monoclinic $P2_1/c$ space group (Table S2), exhibiting the same $[2 \times 2]$ grid topology. In this case, however, the number of tetrafluoroborate anions is reduced to four, implying the deprotonation of altogether four hydrazone sites of the grid ligands to give $[\text{Fe}_4(\text{HL})_4](\text{BF}_4)_4 \cdot 12\text{MeCN}$ (**Fe-4H**, top part of Figure 2 and Figure S4). At this temperature, the four iron metal ions are crystallographically independent. One of them (Fe3) is disordered over two positions (Fe3a and Fe3b, respectively) as well as the two coordinating ligands surrounding this Fe site. The tetrafluoroborate (disordered over two positions) and acetonitrile molecules are located in the lattice void space. The number of solvent molecules was estimated from the electronic density and void space volume calculated by PLATON. Remarkably, the arrangement of the half-deprotonated ligands leads to Fe1 and Fe3 sites surrounded by two deprotonated hydrazone groups, while the pockets surrounding Fe2 and Fe4 centers feature only non-deprotonated hydrazone group. Confirming the trend observed in the previous structures, the short Fe-N bond distances for the iron metal ions within the deprotonated hydrazone environments suggest a LS configuration (1.840(7) – 2.036(5) Å, 1.882(13) – 2.206(10) Å and 1.875(13) – 2.126(12) Å for Fe1, Fe3a and Fe3b respectively, Table S5). It should be noted that the high value observed for one of the distances surrounding Fe3 ions is probably induced by the disorder observed in this metal site. In contrast, the values observed for the metal ions surrounded by coordinating pockets featuring only non-deprotonated hydrazone groups point rather to a HS configuration at 120 K (2.086(6) – 2.190(6) Å and 2.086(6) – 2.197(6) Å for Fe2 and Fe4, respectively, Table 1 and Table S5) even if at this temperature a spin state disorder on these sites is likely to be present. As expected, each NH group of the ligand interacts with one BF_4^- anion through hydrogen bonding. In contrast, no H-donor species were found surrounding the deprotonated hydrazone moieties.

(d) The **Zn-4H** analogue was prepared as a reference complex by replacing iron(II) with zinc(II), in order to analyze the deprotonation pattern observed for **Fe-4H**. Single crystals of **Zn-4H** were obtained as crystalline red plates by diffusion of diethylether into the acetonitrile solution of the complex (see supporting information). The X-ray diffraction data on a single crystal were collected at 120 K and solved in the tetragonal $P4/ncc$ group (Table S6), yielding a $[2 \times 2]$ grid-like complex similar to **Fe-4H**. The presence of four tetrafluoroborate anions confirms the half deprotonation of the four ligands wrapping the **Zn-4H** grid complex: $[\text{Zn}_4(\text{HL})_4](\text{BF}_4)_4 \cdot 8\text{H}_2\text{O}$ (bottom part of Figure 2 and Figure S5). The zinc $[2 \times 2]$ grid is geometrically more distorted than the **Fe-4H** analogue, but is also more crystallographically symmetrical, as the asymmetric unit contains only one ligand and one zinc center (Zn-N: 2.075 – 2.261 Å). The tetrafluoroborate and water molecules are located in the lattice. The number of solvent molecules was estimated from the electronic density and void space volume calculated by PLATON. The good refinement of the structure and its high symmetry demonstrate that the deprotonation pattern for the **Zn-4H** grid is different from that of **Fe-4H**. Indeed, the four Zn^{II} sites are surrounded by two **HL** ligands

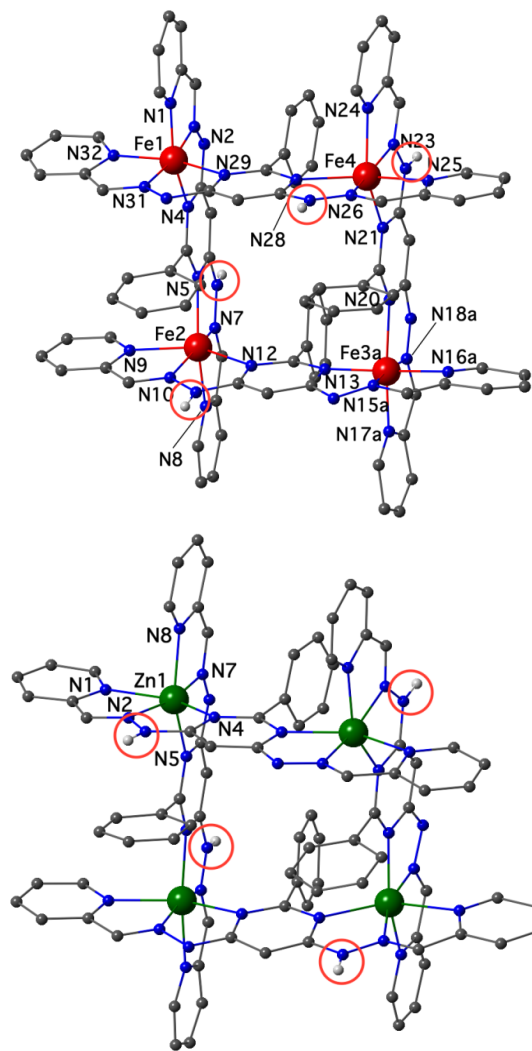


Figure 2. Ball and stick representations of the crystal structures of $[\text{Fe}_4(\text{HL})_4](\text{BF}_4)_4 \cdot 12\text{MeCN}$ complex, **Fe-4H**, (top) and $[\text{Zn}_4(\text{HL})_4](\text{BF}_4)_4 \cdot 8\text{H}_2\text{O}$ complex, **Zn-4H**, (bottom) at 120 K. Fe, Zn, N, C and H atoms are shown in red, green, blue, grey and white, respectively. All non-NH hydrogen atoms, acetonitrile and tetrafluoroborate molecules are omitted for clarity. Non-deprotonated NH sites are circled in red. Only one position for Fe3 (Fe3a) and its corresponding donor atoms are shown.

forming a coordination pocket with one deprotonated and one protonated hydrazone group.

(e) The fully protonated $\text{Zn}^{\text{II}}_4 [2 \times 2]$ grid, **Zn-8H**, was also obtained and structurally characterized by X-ray diffraction (Table S6, Figures S6 and S7). Both Zn^{II} grids, **Zn-4H** and **Zn-8H**, exhibit similar octahedrity values ($S(O_h)$, see below)¹⁸ to the corresponding Fe^{II} grids (Table S7).

Determination and Analysis of the Magnetic Properties of the $\text{Fe}^{\text{II}}_4 [2 \times 2]$ Grid Complexes. Magnetic susceptibility measurements were performed for the **Fe-8H**, **Fe-6H**, and **Fe-4H** complexes in the temperature range of 1.85 - 300 K (Figure 3). The magnetic measurements shown in Figure 3 are reproducible below 300 K for **Fe-8H** and **Fe-4H** while for **Fe-6H**, the temperature cannot be increased above 270 K without losing the complete reversibility. The lack of reversibility is clearly linked to the partial loss of the acetonitrile molecules during the magnetic measurements. Therefore, only perfectly reversible magnetic data corresponding to the structurally characterized materials are discussed in the following. The χT products at highest accessible temperature for

Fe-8H, **Fe-6H**, and **Fe-4H** (300, 270 and 300 K) are 6.6, 4.3 and 3.6 $\text{cm}^3 \text{K mol}^{-1}$, respectively. These values are intermediate between the ones expected for a fully high spin $[\text{Fe}^{\text{HS}}]_4$ complex (12-16 $\text{cm}^3 \text{K mol}^{-1}$; Fe^{HS} : $S = 2$ and $g \approx 2.0$ to 2.3, Curie constant of 3-4 $\text{cm}^3 \text{K mol}^{-1}$) and for a diamagnetic $[\text{Fe}^{\text{LS}}]_4$ species (Fe^{LS} $S = 0$, Curie constant of 0 $\text{cm}^3 \text{K mol}^{-1}$). Upon decreasing the temperature, the χT product gradually decreases reaching to a plateau below 120 K at 2.4, 1.5 and 2.6 $\text{cm}^3 \text{K mol}^{-1}$ for the **Fe-8H**, **Fe-6H** and **Fe-4H** grids, respectively. Analyzing the temperature dependence of the susceptibility, the proportions of HS Fe^{II} centers are estimated at 48, 31 and 26 % at room temperature (taking a g factor of 2.15), and as 17, 11 and 19 % at 50 K, for **Fe-8H**, **Fe-6H** and **Fe-4H** respectively. This behavior clearly demonstrates an incomplete SCO for these complexes that never reach a fully low spin configuration (four Fe^{II} LS sites) at low temperatures and neither a fully high spin configuration (four Fe^{II} HS sites) before desolvation/decomposition of the material at high temperature. This result is also in agreement with the crystal structure analysis (*vide supra*), which indicates the systematic presence of spin state disorder on the Fe2 and Fe4 sites at 120 K for the three compounds (Table 1) and the absence of a high-spin configuration at 290 K. When the temperature is decreased below 20 K, a decrease in the χT product is also observed, indicating most likely the presence of spin-orbit coupling expected for Fe^{II} centers in an octahedral coordination sphere, and possibly intramolecular antiferromagnetic coupling between the Fe^{II} through the pyrimidine groups.¹⁹

The field dependence of the magnetization for the $[2 \times 2]$ Fe^{II}_4 grid (Figures S8-S10) has some notable characteristics: (i) the steady increase of

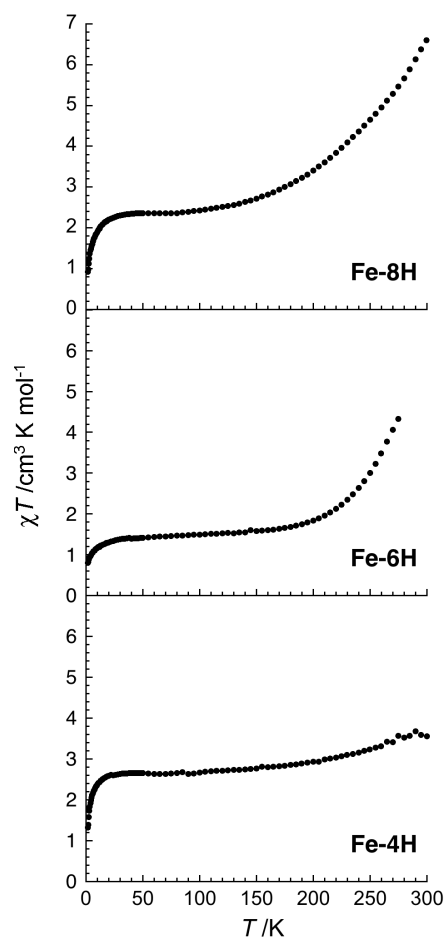


Figure 3. Temperature dependence of χT product at 0.1 (between 1.85 and 50 K) and at 1 T (above 50 K) between 1.85 and 300 K for polycrystalline samples of **Fe-8H**, **Fe-6H**, and **Fe-4H** (where χ is the magnetic susceptibility equal to M/H per mole of $[2 \times 2]$ Fe_4 grid).

the magnetization at low field without inflexion point (“S” shape curve) suggests the absence of significant magnetic interactions between the remaining magnetic sites; and (ii) a linear increase without clear saturation even at 1.8 K under 7 T. This high field behavior of the magnetization and the non-superimposable M vs H/T curves reveal most likely the presence of magnetic anisotropy expected for Fe^{II} HS centers. The magnetization value obtained at 1.85 K under 7 T are 1.95, 1.25 and 2.47 μ_B , confirms the residual presence of Fe^{II} HS ions in **Fe-8H**, **Fe-6H** and **Fe-4H** grid respectively. It is worth mentioning that preliminary solid-state reflectivity measurements on these three complexes indicate the absence of bulk photoactivity at 10 K and thus the impossibility to convert LS Fe^{II} centers into HS ones using light irradiation in the visible range.

UV-Vis Spectroscopic Properties of the Fe^{II}₄ [2×2] Grid Complexes upon Base Titration

The UV-Vis spectra of the grid **Fe-8H** (Figure 4) were measured in acetonitrile/chloroform (1:1) on addition of increasing equivalents of bis(dimethylamino)naphthalene (DMAN) base. The grid **Fe-8H** exhibits an absorption band at 372 nm, which is characteristic of the fully protonated grid complex. When two equivalents of base are added to give **Fe-6H**, the intensity of the band at 455 nm increases but diminishes after further base addition. A third band at 543 nm appears after adding more than 2 base equivalents, increasing in intensity until reaching a maximum intensity for the fully deprotonated species **Fe-0H**. Considering the ratio of molar absorption coefficient and the λ_{\max} obtained, and comparing it to the values known for [Fe(Hpaphy)₂]²⁺ and [Fe(paphy)₂] (Table S8, Hpaphy = pyridine-2-aldehyde-2-pyridylhydrazine), these charge transfer bands observed appear to be of MLCT (Metal Ligand Charge Transfer) type.¹⁴ The deprotonation affects markedly the color of the solution (Figure 4). UV-Vis spectra have also been measured between pH = 1 and pH = 13 in a 50:50 (v/v) mixture of acetonitrile and Britton-Robinson buffer, showing similar results (Figure S11).

¹H NMR Spectral Studies of the Fe^{II}₄ [2×2] Grid Complexes upon Acid/Base Titration. SCO phenomena have been observed in solution by ¹H NMR spectroscopy for Fe^{II}₄ [2×2] grid-type complexes,²⁴ but remain scarce.^{2b,20} Mass spectrometry (see supporting information) was used to ensure that the species in solution were indeed the [2×2] grid structures observed in the solid state (Figures S12-S17). The titration of a solution of **Fe-8H** (followed by ¹H NMR in CD₃CN/CDCl₃ (1:1) at 25°C) with successive equivalents of DMAN or proton sponge showed

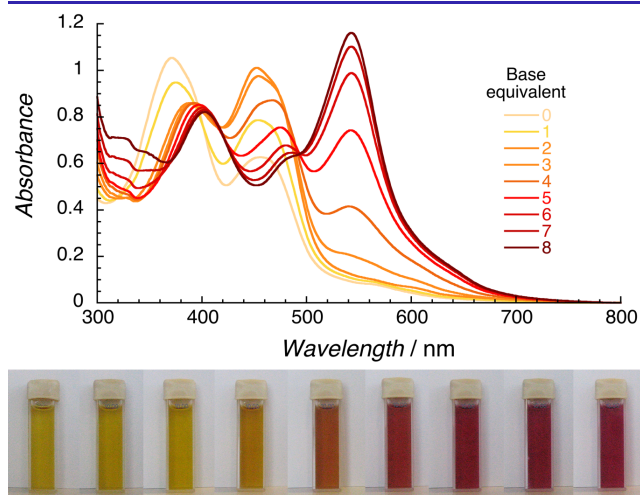


Figure 4. (top) UV-Vis spectra of the grid **Fe-8H** after progressive addition of base in acetonitrile/chloroform (1:1); (bottom) corresponding pictures of **Fe-8H** solution after addition of base (0 to 8 eq, left to right).

chemical shifts ranging from around -40 to 200 ppm, with broad signals, and a shift of the signals towards the range for diamagnetic species as more equivalents of base were added (Figure S18). The titration produced a color change of the solution, from yellow to dark red (Figure 4, bottom), as well as a change in the solubility of the **Fe-nH** complex. The **Fe-8H** grid is soluble in acetonitrile but not in chloroform, whereas the opposite is true for **Fe-0H**. Hence the solvent mixture CD₃CN/CDCl₃ (1:1) was chosen for the NMR studies. The titration was also done in pure CD₃CN (0 to 4 equivalents of base, up to the solubility limit) to allow for an increase in the maximum concentration in order to give a better NMR spectrum (Figure S19). The amount of exchange present in solution, known for grid structures,^{13c} plus the equilibrium between **Fe-nH** species, render complicated the observation of the paramagnetic peaks associated with the grid (Figures S18 and S19). Nevertheless, paramagnetic peaks are clearly observed for **Fe-8H** to **Fe-4H**, as expected from the crystal structures, and are in agreement with the presence of HS Fe^{II} centers in the grid complexes. The titration also follows the expected trend, going from a strongly paramagnetic species for **Fe-8H** to a weakly paramagnetic **Fe-4H** system (containing less HS Fe^{II} sites), then to LS diamagnetic **Fe-2H** to **Fe-0H** grids with no paramagnetic signal observed. The formally **Fe-3H** complex is the crossover species between paramagnetic and diamagnetic systems, and it is difficult to infer whether or not this species is still paramagnetic in solution.

To further investigate this magnetic behavior in solution upon deprotonation, the magnetic susceptibility was determined by ¹H NMR using the Evans method on the **Fe-8H** grid following the same titration procedure. The results obtained (Figure 5) agree completely with those qualitatively described above. The susceptibility value for **Fe-8H** is 0.047 cm³ mol⁻¹ ($\chi T = 14$ cm³ K mol⁻¹) in excellent agreement with the presence of four Fe^{II} HS (with $g = 2.16$). Therefore, in solution, the **Fe-8H** complex is, or is close to, the fully paramagnetic configuration. Progressive addition of up to 8 equivalents of DMAN produced a marked decrease of the magnetic susceptibility to 0 cm³ mol⁻¹ between 5 and 6 equivalents of base (Figure 5). This decrease of the susceptibility on addition of base clearly revealed a dependence of the grid magnetic configuration with a number of HS or LS Fe^{II} sites dependent upon the degree of deprotonation. Furthermore, back titration performed by adding progressively trifluoromethanesulfonic acid (CF₃SO₃H) resulted in a similar pattern for the magnetic susceptibility, showing the reversibility of this system upon protonation/deprotonation. This result also highlights the fully diamagnetic configuration in solution for species **Fe-2H** to **Fe-0H**. Here again it is difficult to be definitive about the magnetic state of **Fe-3H**, which seems to be still slightly paramagnetic but falls within the standard deviation range of diamagnetic species (Figure 5). On the

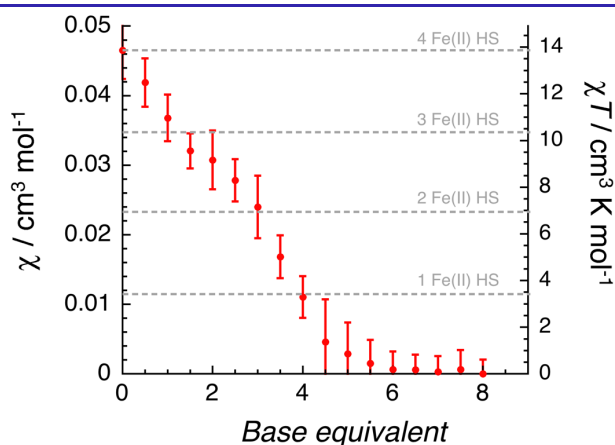


Figure 5. Evolution of the magnetic susceptibility (and χT product) of **Fe-nH** in CD₃CN/CDCl₃ (1:1) at 298 K on titration with DMAN base as observed by ¹H NMR using the Evans method. Error bars represent standard deviation over 3 experiments.

other hand, the formally **Fe-4H** complex generated by adding four base equivalents is clearly not diamagnetic suggesting that the deprotonation of the four hydrazone groups does not lead to four LS Fe^{II} sites in agreement with the structural and magnetic measurements in solid state (Table 1). The present titration results demonstrate a reversible Proton-Driven Spin State Switching (PD-SSS) without modification of the metal ion coordination in contrast to what has been observed in the tris(bipyridine)iron(II) system which shows also a proton-driven spin state switching but induced by a change in coordination state upon protonation (PD-CISSS).^{17a}

The [2×2] grid **Zn-8H** was also investigated as a diamagnetic model for **Fe-8H**. The base chosen for this titration was triethylamine (NEt₃) to make sure that the base signals would not interfere with the diamagnetic grid signals. As in the case of **Fe-8H**, the solubility of the grid changes with deprotonation, with **Zn-8H** to **Zn-4H** being soluble in acetonitrile (Figure S20), and **Zn-3H** to **Zn-0H** being soluble in DMSO but not in acetonitrile or chloroform (Figure S21). In contrast to the iron grid, all ¹H NMR signals of **Zn-8H** correspond as expected to a diamagnetic species over the titration range (from 0 to 8 equivalents of base) and can be assigned by COSY NMR (Figure S22). Both **Fe-4H** and **Zn-4H** seem to be pivotal species in their respective deprotonation series, as going from the **4H** to **3H** protonation states shows similar changes both in solubility and color.

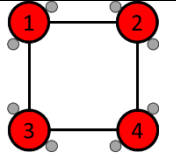
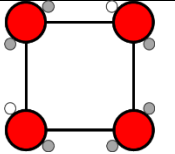
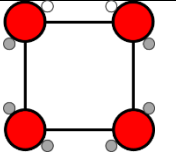
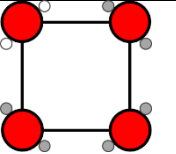
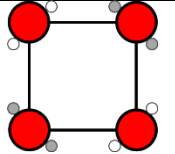
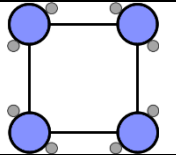
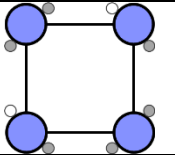
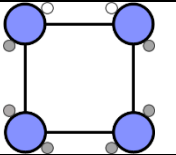
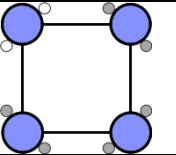
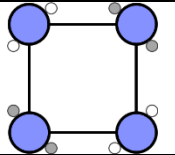
As crystal structures only reflect the solid state and not the solution state observed by ¹H NMR, control experiments have been performed. In the case of the Fe complexes, two distinct ¹H NMR spectra were observed during the titration, the initial one being the same as that of a solution obtained by dissolution of **Fe-8H** crystals (Figures S18 and S19). After addition of 4 equivalents of base, the second distinct pattern was identified. This solution was then taken out of the NMR spectrometer and slow ether diffusion yielded crystals confirmed by X-Ray crystallography to be **Fe-4H**. To ensure that the crystals obtained were the only type present, several different crystals were tried, giving the same result. Therefore, the symmetrical deprotonation pattern observed for the **Zn-4H** grid (consisting of each metal ion site surrounded by two HL ligands forming a coordination pocket with one deprotonated and one non-deprotonated hydrazone group) is not observed for **Fe-4H** even after crystallization of the titrated solution. This result is consistent with the paramagnetic signature of the **Fe-4H** solution (Figure 5) as one would expect a symmetrical **Fe-4H** species to be fully diamagnetic with each Fe^{II} center surrounded by one deprotonated ligand environment. It is worth mentioning that **Zn-4H** with the symmetrical deprotonation pattern has also been reproducibly isolated from the corresponding titrated NMR solution.

Computational studies on Fe^{II} grids: Magnetic Configuration Energetics and Deprotonation Patterns. In order to investigate how the successive deprotonation of the bridging ligands affects the SCO properties within the grid, DFT computations have been performed to monitor the stability of the relevant magnetic configurations depending on the deprotonation pattern. These configurations are **HS** with four HS Fe^{II} sites, **LS** with four LS Fe^{II} sites and intermediate states with two HS and two LS Fe^{II} centers either in opposite, noted **IS-trans**, or neighboring, noted **IS-cis**, sites of the grid, or with one HS and three LS Fe^{II} centers referred to **HLLL** (Table S9). Other magnetic configurations have been computed and found of little interest for the discussion. The stability is discussed only in terms of electronic enthalpies (H_{elec}) due to the difficulty to evaluate the vibrational enthalpy (H_{vib}) and entropy (S_{vib}) contributions. The H_{elec} values for relevant magnetic configurations and deprotonation patterns of **Fe-8H**, **Fe-6H**, **Fe-4H** and **Fe-3H** are given in Table S9. To evaluate the magnetic configuration stability at a given temperature from our calculations and allow a direct comparison with experiment, we have assumed $\Delta H_{vib} = -3$ kJ/mol, and $\Delta S_{tot} = 35$ J/K·mol, which lie in the common range of values, and a Boltzmann

distribution of states based on free enthalpies ($\Delta G = \Delta H_{elec} + \Delta H_{vib} - T\Delta S_{tot}$). The computational model consists of an isolated [2×2] grid, whose structure is optimized at different magnetic configurations to obtain H_{elec} . Deviations from experimental measurements can be ascribed to crystal packing effects originated in the interactions with counterions, solvent molecules or other grids. These effects could be incorporated to our computational analysis by means of solid-state calculations with periodic boundary conditions. However, the size of the unit cells (ca. 1000 atoms) makes such analysis extremely expensive in the present case.

The calculations for the **Fe-8H** complex indicate a **HS** ground configuration with a less stable **LS** state lying at about 21.1 kJ/mol (see Table S9), and also a **IS-trans** state that is slightly preferred over the **IS-cis** one (7.3 and 8.9 kJ/mol above **HS**, respectively). One of the reasons for the disfavored **LS** structure in the calculations is found by looking at the Fe^{II} coordination spheres. Indeed, most of the LS Fe^{II} centers in the structurally characterized grids (shown in Tables 2 and S7) have octahedricity values within the range 2.24-2.46 indicating a slightly distorted octahedral geometry.^{17,22} In contrast, the **LS** configuration for **Fe-8H** has a significantly larger calculated $S(O_h)$ value (ca. 2.60; Table S10) indicating that the Fe coordination sphere should be more distorted and, thus, disfavored. In the case of the **Fe-6H** complex, three deprotonation patterns have been explored: a single deprotonation of two different Fe centers in (i) **cis** and (ii) **trans** positions within the grid, or (iii) a double deprotonation in one center (*i.e.* **homo**). The results show that such **homo** pattern is clearly unfavorable with respect to the **cis** and **trans** ones, both showing similar stability. In light of these calculations, it is difficult to suggest which might be the most stable structure at room temperature, since multiple configurations should be thermally accessible. To illustrate the complexity, assuming the aforementioned ΔH_{vib} and ΔS_{tot} values, there would be four states with more than 5% population at 300 K, and the ratio of **HS:IS:LS** states would be ca. 1:1:0. This is in line with the poorly-defined ¹H NMR spectrum following the addition of two equivalents of base as observed in Figures S18 and S19, indicative of a superposition of multiple proton-transfer isomers. Similarly, at 120 K the ratio of **HS:IS:LS** states would be of ca. 1:9:0. For **Fe-4H**, we have explored two deprotonation patterns in which only one proton is removed from each of the four Fe^{II} centers (so-called **hetero**) or two protons are removed from the same two Fe^{II} centers (*i.e.* **homo**). In contrast with the results discussed for **Fe-6H**, the **homo** pattern is far more stable than the **hetero** one for all of the explored magnetic configurations. Concerning the stability, the **LS** configuration is the most stable one in terms of H_{elec} , but the **IS-trans** lies very close in energy (1.0 kJ/mol) so it is likely thermally populated at moderate temperatures due to the favorable entropic contribution. Indeed, assuming the same ΔH_{vib} and ΔS_{tot} values as before, we would obtain a population of 93% of the **IS-trans** state at 120 K with the **homo** deprotonation pattern, which would be consistent with the crystallographic data (Table 1). Finally, for **Fe-3H** we have performed a less systematic study, whose purpose has been to evaluate (i) the preference for the **homo** deprotonation over the **hetero** one, and (ii) the possibility of accessible paramagnetic configurations. The two points are confirmed by our calculations; the **hetero** configuration lies 8 kJ/mol above the **homo** one, and the **HLLL** state is accessible since it is only 1.3 kJ/mol higher than the **LS** state, which means that at room temperature one would have 70% of **HLLL** state. These results are also in good agreement with the experimental data shown in Figure 5. Overall, the calculations clearly over-stabilize the **HS** configuration for the **Fe-8H** grid (8+ charge), and to some extent also for the **Fe-6H** grids (6+ charge). In turn, the **HS/LS** stability in the **Fe-4H** grids (4+ charge) seems to be better balanced. The origin for such decreasing error as we reduce the intrinsic charge of the grid might be associated to the decrease of the intermolecular interactions between the grids and their neighbors (either counterions, lattice-solvent molecules or other grids).

Table 2. Calculated octahedricity parameters: $S(O_h)$ values^{18,22} as a measure of distortion of the Fe-N₆ coordination sphere for 1 to 4 SCO centers in selected grids. Values of $S(O_h)$ smaller than 4.42 indicate a geometry closer to the octahedron than to the trigonal prism, while $S(O_h)$ values above 4.42 point toward a distorted trigonal prism geometry.^{18,22}

Deprotonation		Fe-8H	Fe-6H-Trans	Fe-6H-Cis	Fe-6H-Homo	Fe-4H-Homo
HS						
$S(O_h)$	①	6.44	6.47	6.36	6.45	6.61
	②	6.51	6.77	7.07	6.58	6.58
	③	6.58	6.75	7.09	6.91	6.53
	④	6.46	6.46	6.50	6.48	6.62
	Avg.	6.50	6.61	6.76	6.61	6.58
LS						
$S(O_h)$	①	2.58	2.39	2.45	2.40	2.32
	②	2.60	2.41	2.45	2.42	2.41
	③	2.60	2.45	2.38	2.39	2.44
	④	2.58	2.42	2.40	2.40	2.28
	Avg.	2.59	2.42	2.42	2.40	2.36

Indeed, these interactions might have an important electrostatic contribution that is missing in our calculations, whose importance must certainly decrease along with the deprotonation. If this contribution were stabilizing the **LS** state (or penalizing the **HS** state), then the apparent errors in the mixed **HS/LS** state stability could be certainly ascribed to the absence of such electrostatic interactions in our computational model. Nevertheless, the deprotonation patterns observed by crystallography are supported by the present calculations, with the first two deprotonation steps (**Fe-8H** to **Fe-6H**) occurring in opposite sides of the grid (*i.e.* *hetero*) and the third and fourth steps (**Fe-6H** to **Fe-4H**) occurring in the already-deprotonated sites (*i.e.* *homo*).

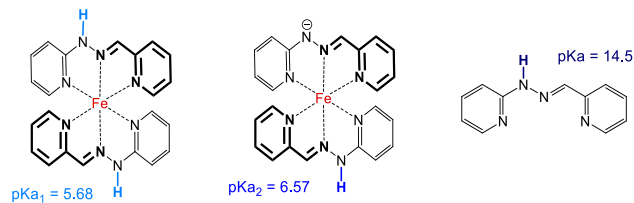
Additional pKa calculations have been performed on a truncated version of an isolated Fe^{II} center (see [supporting information](#)). The numerical results show that the HS Fe^{II} center has a higher pKa value than the LS site (Table S11). Overall the unexpected unsymmetrical deprotonation pattern seen in **Fe-4H** seems to be induced by the intramolecular cooperativity enforced by the ligands, as has been shown for similar Fe^{II} [2×2] grids, both experimentally and theoretically.^{12a,21} This effect can be monitored by Continuous Shape Measurements (CShM), which evaluate the octahedricity of the Fe-N₆ coordination sphere, *i.e.* its distortion from an ideal octahedron ($S(O_h) = 0$),^{18,22} and enable us to gain some relevant insight concerning the mutual influence between the Fe^{II} centers in the studied grid (Table 2). First, the deprotonation of one coordination pocket not only affects the $S(O_h)$ value of the Fe metal ion in that pocket but affects also the two neighboring Fe centers coordinated to the two ligands of the deprotonated coordination pocket and, indirectly, the whole grid. This is precisely what is expected from a system displaying intramolecular cooperativity, and can be illustrated, for instance, in the $S(O_h)$ values of the **HS** configuration for the **Fe-6H-Cis** deprotonation pattern, in which the largest value corresponds to an Fe pocket that is not deprotonated (7.09, Table 2). This is surprising at first sight, but can be understood by looking at the actual structure of the grid, which presents a significant degree of distortion that stems from the Fe-N₆ coordination sphere but is absorbed by the whole grid. As a result of this observation and for the sake of simplicity, our discussion in the next paragraph will be based on $S(O_h)$ values averaged for the four

Fe sites of the grid (see Avg. values in Tables 2 and S10). Indeed, the deprotonation affects differently the HS and LS Fe^{II} centers. The $S(O_h)$ value of HS centers increases from **Fe-8H** (6.50) to **Fe-6H** (6.61 for *homo* and *trans*, and 6.76 for *cis*) and then decreases from **Fe-6H** to **Fe-4H** (6.58). On the contrary, the $S(O_h)$ value of the LS centers continuously decrease upon deprotonation from **Fe-8H** (2.59) to **Fe-6H** (2.42 for *trans* and *cis*, and 2.40 for *homo*) to **Fe-4H** (2.36) (Tables 2 and S10). This observation indicates that the coordination pockets of the ligand are better suited to coordinate a LS Fe^{II} metal ion after deprotonation, whereas the opposite trend holds for a HS center. Making the fair assumption that, the larger the distortion of the Fe-N₆ sphere, the larger the energy penalty, it would explain the progressive (de)stabilization of (HS)LS centers upon deprotonation that is captured in Table S9. Of course, the scenario is significantly more complex for **IS** and **HLLL** configurations so we have restricted our analysis to states in which all Fe centers are either HS or LS (Table S10). Even though other energy contributions are likely to contribute to the HS/LS relative stability, this analysis provides a microscopic interpretation to the magnetic configuration stability of the reported [2×2] grid.

Modulation of the magnetic configuration in the [Fe₄(H_nL₄)]⁽ⁿ⁾⁺ (n = 4, 6, 8) complexes as a function of protonation state in light of the structural, magnetic and computational data. Remarkably, on reaching the conditions for deprotonation of four of the eight hydrazone N-H sites belonging to the four ligands of the [Fe₄(H₂L)₄]⁸⁺ complex (**Fe-8H**), the crystal structure of the corresponding complex [Fe₄(HL₄)₄]⁴⁺ (**Fe-4H**) showed that a double deprotonation had occurred at two Fe^{II} metal centers (Figure 2, top), the other two coordination centers remaining fully protonated. This result is in strong contrast with an expected symmetrical pattern of single deprotonation on each of the four coordination sites, as it is indeed observed in the crystal structure of the zinc analogue **Zn-4H** (Figure 2, bottom). Indeed, it was shown that for complexes of a ligand such as **Hpaphy** (Scheme 2), the pKa increases after the first ligand deprotonation.¹⁴ An estimation of the acidity of the N-H site for **Hpaphy** gives pK_a = 14.5.²³ In the [Fe^{II}(Hpaphy)₂]²⁺ complex, the N-H site becomes much more acidic, due to the binding of the

doubly charged metal cation ($pK_{a1} = 5.68$). The second deprotonation occurs at a higher pK_{a2} of 6.57 in aqueous solution (Scheme 2).¹⁴ These values offer an approximation of what one would expect for the iron(II) sites of the **Fe-8H** grid. Interestingly both $[\text{Fe}(\text{Hpaphy})_2]^{2+}$ and $[\text{Fe}(\text{paphy})_2]$ species are diamagnetic complexes.²⁴

Scheme 2. Acidity constants pK_a of $[\text{Fe}(\text{Hpaphy})_2]^{2+}$ (left), $[\text{Fe}(\text{Hpaphy})(\text{paphy})]^+$ (middle) and **Hpaphy (right).**



As stated above, **Fe-8H** exhibits a very unusual deprotonation behavior. As for **paphy** complexes, two different pK_a s would be expected on the same metal center, $pK_{a1}(\text{H}_2\text{L}/\text{HL})$ and $pK_{a2}(\text{HL}/\text{L})$, leading to the deprotonation pattern indeed observed for **Zn-4H**. The proposed explanation for the different deprotonation patterns observed for **Fe-4H** and **Zn-4H** is that the Fe^{II} spin state switching from HS to LS affects the pK_a of the corresponding N-H ligand site to a point that the $pK_{a2}(\text{HL}/\text{L})$ of an LS coordination center becomes lower than the $pK_{a1}(\text{H}_2\text{L}/\text{HL})$ of a HS site. Following this reasoning, **Fe-6H** then also exhibits an interesting deprotonation pattern, as in that case a *trans* deprotonation is observed involving two different, diagonally located Fe^{II} centers – as opposed to the removal of both protons on the same metal site. This cooperative effect between Fe^{II} centers due to ligand rigidity within iron(II) $[2 \times 2]$ grids has been evidenced before for multi-step spin crossover processes, both experimentally and theoretically.^{12a,21} These results show that the SCO is facilitated first between Fe^{II} from opposite corners but then hampered for further spin state switching. The experimental and theoretical data on our system lead us to similar conclusion on the importance of cooperativity and ligand rigidity in a grid complex, as evidenced by the CShM calculations (Table S10). DFT calculations also showed clearly that for a same ligand system, the pK_a is lower for a LS Fe^{II} site than it is for the HS analogue (Table S11). Relating the results of the calculations to the behavior of our system, the first double deprotonation step (**Fe-8H** to **Fe-6H**), rather than resulting from the influence of the Fe^{II} spin state on the ligand pK_a , is governed by the rigidity of the ligand which forces a deprotonation on two different sites. The second double deprotonation step (**Fe-6H** to **Fe-4H**) is in turn governed by the change in pK_a induced by the SCO of the trans-located iron centers, now in the LS state. The reason is that the pK_{a1} of the two remaining HS iron centers must be higher than the pK_{a2} of the two LS iron centers that underwent SCO. The stability of this unsymmetrical deprotonation pattern for **Fe-4H** is well supported by the calculations on both grid stability and influence of Fe^{II} spin state on pK_a (Tables 2 and S11).

CONCLUSIONS

The data presented herein demonstrate the possibility of modulating the spin state of the Fe^{II} sites and subsequently the magnetic properties of a $[2 \times 2]$ Fe^{II} grid-like complex by variation of the degree of deprotonation of the hydrazine-based N-H sites of the ligand in the complex. Evidence has been provided, both in the solid state and in solution, towards understanding the strong influence of the spin-crossover process on the pK_a s of the grid ligands, which exhibit a unique deprotonation pattern. The present study provides a demonstration of the effect of spin state switching of a chemical property, here on ligand pK_a in a metallosupramolecular grid.

ASSOCIATED CONTENT

Supporting Information

The Supporting Information is available free of charge on the ACS Publications website at DOI:

Experimental details about syntheses, crystal structures, physical characterizations and theoretical calculations (PDF)

X-ray crystallographic data for **Fe-8H** (120 and 290 K; CIF), **Fe-6H** (120 and 290 K; CIF), **Fe-4H** (120 K; CIF), **Zn-8H** (173 K; CIF) and **Zn-4H** (120 K; CIF)

AUTHOR INFORMATION

Corresponding Authors

* clerac@crpp-bordeaux.cnrs.fr

* lehn@unistra.fr

ORCID

Sébastien Dhers: 0000-0001-5530-0818

Abhishake Mondal: 0000-0002-5061-2326

David Aguilà: 0000-0001-8707-7833

Juan Ramirez: 0000-0003-2254-5813

Sergi Vela: 0000-0002-3431-2470

Pierre Dechambenoit: 0000-0001-7850-2260

Jonathan R. Nitschke: 0000-0002-4060-5122

Rodolphe Clérac: 0000-0001-5429-7418

Jean-Marie Lehn: 0000-0001-8981-4593

Notes

The authors declare no competing financial interests.

ACKNOWLEDGMENTS

We thank the ERC (Advanced Research Grant SUPRADAPT 290585), the University of Strasbourg, the University of Bordeaux, the Région Nouvelle Aquitaine, the CNRS, the GdRMCM-2: Magnétisme et Commutation Moléculaires and the MOLSPIN COST action CA15128 for funding. S.V. is thankful to the LabEx-Chemistry of Complex Systems for a post-doctoral grant (ANR-10-LABX-0026CSC) and to the regional High-Performance Computing (HPC) center in Strasbourg for computational resources. J.M.L. thanks Jack Harrowfield and Mihail Stadler for discussions.

REFERENCES

- (a) Kahn, O.; Martinez, C. J. *Science* **1998**, 279, 44-48. (b) Gatteschi, D.; Sessoli, R.; Villain, F. *Molecular Nanomagnets*, Oxford University Press: Oxford, U.K., **2006**. (c) Li, J.-R.; Kuppler, R. J.; Zhou, H.-C. *Chem. Soc. Rev.* **2009**, 5, 1477-1504. (d) Chen, L.; Luque, R.; Li, Y. *Chem. Soc. Rev.* **2017**, 46, 4614-4630.
- (a) Breuning, E.; Ruben, M.; Lehn, J.-M.; Renz, F.; Garcia, Y.; Ksenofontov, V.; Gütllich, P.; Wegelius, E.; Rissanen, K. *Angew. Chem.* **2000**, 112, 2563-2566; *Angew. Chem. Int. Ed.* **2000**, 39, 2504-2507. (b) Ruben, M.; Breuning, E.; Lehn, J.-M.; Ksenofontov, V.; Renz, F.; Gütllich, P.; Vaughan, G. B. M. *Chem.-Eur. J.* **2003**, 9, 4422-4429.
- Matsumoto, T.; Newton, G. N.; Shiga, T.; Hayami, S.; Matsui, Y.; Okamoto, H.; Kumai, R.; Murakami, Y.; Oshio, H. *Nat. Commun.* **2014**, 5, 3865.
- Seredyuk, M.; Znovjyak, K. O.; Kusz, J.; Nowak, M.; Muñoz, M. C.; Real, J. A. *Dalton Trans.* **2014**, 43, 16387-16394.
- (a) Galet, A.; Gaspar, A. B.; Muñoz, M. C.; Burkin, G. V.; Levchenco, G.; Real, J. A. *Adv. Mater.* **2005**, 17, 2949-2953. (b) Gütllich, P.; Goodwin, H. A. *Spin Crossover in Transition Metal Compounds I*, Eds: Topics in Current Chemistry, Vol 233, Springer, Berlin **2004**. (c) Gütllich, P.; Goodwin, H. A. *Spin Crossover in Transition Metal Compounds II*, Eds: Topics in Current Chemistry, Vol 234, Springer, Berlin **2004**. (d) Gütllich, P.; Goodwin, H. A.

Spin Crossover in Transition Metal Compounds III, Eds: Topics in Current Chemistry, Vol 235, Springer, Berlin **2004**. (e) Halcrow, M. A. ed., *Spin-Crossover Materials*, John Wiley & Sons Ltd, Chichester, **2013**. (f) Gütlich, P.; Garcia, Y.; Goodwin, H. A. *Chem. Soc. Rev.* **2000**, 29, 419-427. (g) Hardy, J. G. *Chem. Soc. Rev.* **2013**, 42, 7881-7899. (h) Brooker, S. *Chem. Soc. Rev.* **2015**, 44, 2880-2892.

(6) (a) Hanan, G. S.; Volkmer, D.; Schubert, U. S.; Lehn, J.-M.; Baum, G.; Fenske, D. *Angew. Chem. Int. Ed.* **1997**, 36, 1842-1844. (b) Garcia, A. M.; Romero-Salguero, F. J.; Bassani, D. M.; Lehn, J.-M.; Baum, G.; Fenske, D. *Chem.-Eur. J.* **1999**, 6, 1803-1808. (c) Barboiu, M.; Vaughan, G.; Graff, R.; Lehn, J.-M. *J. Am. Chem. Soc.* **2003**, 125, 10257-10265. (d) Onions, S. T.; Frankin, A. M.; Horton, P. N.; Hursthouse, M. B.; Matthews, C. J. *Chem. Commun.* **2003**, 2864-2865. (e) Ruben, M.; Rojo, J.; Romero-Salguero, F. J.; Uppadine, L. H.; Lehn, J.-M. *Angew. Chem. Int. Ed.* **2004**, 43, 3644-3662.

(7) Weissbuch, I.; Baxter, P. N. W.; Cohen, S.; Cohen, H.; Kjaer, K.; Howes, P. B.; Als-Nielsen, J.; Hanan, G. S.; Schubert, U. S.; Lehn, J.-M.; Leiserowitz, L.; Lahav, M. *J. Am. Chem. Soc.* **1998**, 120, 4850-4860.

(8) Breuning, E.; Ziener, U.; Lehn, J.-M.; Wegelius, E.; Rissanen, K. *Eur. J. Inorg. Chem.* **2001**, 1515-1521.

(9) (a) Semenov, A.; Spatz, J. P.; Möller, M.; Lehn, J.-M.; Sell, B.; Schubert, D.; Weidl, C. H.; Schubert, U. S. *Angew. Chem.* **1999**, 111, 2701-2705; *Angew. Chem. Int. Ed.* **1999**, 38, 2547-2550. (b) Ziener, U.; Lehn, J.-M.; Mourran, A.; Möller, M. *Chem.-Eur. J.* **2002**, 8, 951-957.

(10) (a) Ruben, M.; Ziener, U.; Lehn, J.-M.; Ksenofontov, V.; Gütlich, P.; Vaughan, G. B. M. *Chem.-Eur. J.* **2005**, 11, 94-100. (b) Uppadine, L. H.; Gisselbrecht, J.-P.; Kyritsakas, N.; Näntinen, K.; Rissanen, K.; Lehn, J.-M. *Chem.-Eur. J.* **2005**, 11, 2549-2565. (c) Wu, D.-Y.; Sato, O.; Einaga, Y.; Duan, C.-Y. *Angew. Chem.* **2009**, 121, 1503-1506. (d) Wei, R.-J.; Huo, Q.; Tao, J.; Huang, R.-B.; Zheng, L.-S. *Angew. Chem.* **2011**, 123, 9102-9105; *Angew. Chem., Int. Ed.* **2011**, 50, 8940-8943. (e) Li, F.; Clegg, J. K.; Goux-Capes, L.; Chastanet, G.; D'Alessandro, D. M.; Létard, J.-F.; Kepert, C. J. *Angew. Chem.* **2011**, 123, 2872-2875; *Angew. Chem., Int. Ed.* **2011**, 50, 2820-2823. (f) Schneider, B.; Demeshko, S.; Dechert, S.; Meyer, F. *Angew. Chem.* **2010**, 122, 9461-9464; *Angew. Chem., Int. Ed.* **2010**, 49, 9274-9277. (g) Schneider, B.; Demeshko, S.; Neudeck, S.; Dechert, S.; Meyer, F. *Inorg. Chem.* **2013**, 52, 13230-13237.

(11) Stefankiewicz, A. R.; Lehn, J.-M. *Chem.-Eur. J.* **2009**, 15, 2500-2503.

(12) (a) Steinert, M.; Schneider, B.; Dechert, S.; Demeshko, S.; Meyer, F. *Inorg. Chem.* **2016**, 55, 2363-2373. (b) Wang, Y.-T.; Li, S.-T.; Wu, S.-Q.; Cui, A.-L.; Shen, D.-Z.; Kou, H.-Z. *J. Am. Chem. Soc.* **2013**, 135, 5942-5945. (c) Ni, Z.; McDaniel, A. M.; Shores, M. P. *Chem. Sci.* **2010**, 1, 615-621.

(13) (a) Ruben, M.; Lehn, J.-M.; Vaughan, G. *Chem. Commun.* **2003**, 12, 1338-1339. (b) Uppadine, L. H.; Gisselbrecht, J.-P.; Lehn, J.-M. *Chem. Commun.* **2004**, 718-719. (c) Barboiu, M.; Ruben, M.; Blasen, G.; Kyritsakas, N.; Chacko, E.; Dutta, M.; Redekovich, O.; Leton, K.; Brook, D. J. R.; Lehn, J.-M. *Eur. J. Inorg. Chem.* **2006**, 784-792. (d) Tong, J.; Demeshko, S.; Dechert, S.; Meyer, F. *Eur. J. Inorg. Chem.* **2017**, 4333-4343. (e) Schäfer, B.; Greisch, J.-F.; Faus, I.; Bodenstern, T.; Salitros, I.; Fuhr, O.; Fink, K.; Schünemann, V.; Kappes, M. M.; Ruben, M. *Angew. Chem. Int. Ed.* **2016**, 55, 10881-10885.

(14) Green, R. W.; Hallman, P. S.; Lions, F. *Inorg. Chem.* **1964**, 3, 376-381.

(15) From a synthetic point of view, the use of an appropriate base to deprotonate the NH group of the free ligand, transforms this one in a nucleophilic reagent that is possible to alkylate thus opening a synthetic route toward new very diverse ligands. See: Tiemann, P.; Marchal, A.; Lehn, J.-M. *Tetrahedron Lett.* **2005**, 46, 6349-6353.

(16) Hasserodt, J.; Kolanowski, J. L.; Touti, F. *Angew. Chem.* **2014**, 126, 60-75; *Angew. Chem. Int. Ed.* **2014**, 53, 60-73.

(17) (a) Nowak, R.; Prasetyanto, E. A.; De Cola, L.; Bojer, B.; Siegel, R.; Senker, J.; Rössler, E.; Weber, B. *Chem. Commun.* **2017**, 53, 971-974. (b) Gaudette, A. I.; Thorarindottir, A. E.; Harris, T. D. *Chem. Commun.* **2017**, 53, 12962-12965. (c) Touti F.; Maurin, P.; Canaple, L.; Beuf, O.; Hasserodt, J. *Inorg. Chem.*, **2012**, 51, 31-33. (d) Luo, Y.-H.; Nihei, M.; Wen, G.-J.; Sun B.-W.; Oshio, H. *Inorg. Chem.*, **2016**, 55, 8147-8152. (e) Enamullah, M.; Linert, W.; Gutmann, V.; Jameson, R. F. *Monatsh. Chem.*, **1994**, 125, 1301-1309. (f) Enamullah, M.; Linert, W. *J. Coord. Chem.*, **1995**, 35, 325-335.

(18) Alvarez, S.; Avnir, D.; Lluell, M.; Pinsky, M. *New J. Chem.* **2002**, 26, 996-1009.

(19) (a) Lin, P. H.; Smythe, N. C.; Gorelsky, S. I.; Maguire, S.; Henson, N. J.; Korobkov, I.; Scott, B. L.; Gordon, J. C.; Baker, R. T.; Murugesu, M. *J. Am. Chem. Soc.* **2011**, 133, 15806-15809. (b) Pali, A. V.; Clemente-Juan, J. M.; Coronado, E.; Klokishner, S. I.; Ostrovsky, S. M.; Reu, O. S. *Inorg. Chem.* **2010**, 49, 8073-8077. (c) Gomez-Coca, S.; Cremades, E.; Aliaga-Alcalde, N.; Ruiz, E. *J. Am. Chem. Soc.* **2013**, 135, 7010-7018.

(20) (a) Anderson, P. A.; Astley, T.; Hitchman, M. A.; Keene, F. R.; Mobaraki, B.; Murray, K. S.; Skelton, B. W.; Tiekink, E. R. T.; Toftlund, H.; White, A. H. *J. Chem. Soc., Dalton Trans.* **2000**, 3505-3512. (b) Reger, D. L.; Littler, C. A.; Rheringold, A. L.; Lam, M.; Liable-Sands, L. M.; Rhagitan, B.; Concolino, T.; Mohan, A.; Long, G. J.; Brioso, V.; Grandjean, F. *Inorg. Chem.* **2001**, 40, 1508-1520. (c) Weber, B.; Walker, F. A. *Inorg. Chem.* **2007**, 46, 6794-6803. (d) Schlamp, S.; Schulten, J.; Betz, R.; Bauch, T.; Mudring, A. V.; Weber, B. *Z. Anorg. Allg. Chem.* **2012**, 638, 1093-1102. (e) Shakirova, O. G.; Lavrenova, L. G.; Daletsky, V. A.; Shusharina, E. A.; Griaznova, T. P.; Katsyuba, S. A.; Syakaev, V. V.; Skripacheva, V. V.; Mustafina, A. R.; Solovieva, S. E. *Inorg. Chim. Acta* **2010**, 363, 4059-4064. (f) Schlamp, S.; Thoma, P.; Weber, B. *Eur. J. Inorg. Chem.* **2012**, 2759-2768. (g) Rodríguez-Jiménez, S.; Brooker, S. *Inorg. Chem.* **2017**, 56, 13697-13708. (h) Shores, M. P.; Klug, C. M.; Fiedler, S. R. *Spin-state switching in solution, Spin-Crossover Materials*; John Wiley & Sons Ltd: Chichester, England, **2013**, 281-301.

(21) (a) Zueva, E. M.; Ryabikh, E. R.; Kuznetsov, A. M.; Borshch, S. A. *Inorg. Chem.* **2011**, 50, 1905-1913. (b) Zueva, E. M.; Ryabikh, E. R.; Borshch, S. A. *Inorg. Chem.* **2011**, 50, 11143-11151. (c) Borshch, S. A.; Zueva, E. M. *Eur. J. Inorg. Chem.* **2013**, 1009-1014.

(22) Alvarez, S.; Alemany, P.; Casanova, D.; Cirera, J.; Lluell, M.; Avnir, D. *Coord. Chem. Rev.* **2005**, 249, 1693-1708.

(23) (a) Lions, F.; Martin, K. V. *J. Am. Chem. Soc.* **1958**, 80, 3858-3865. (b) Geldard, J. F.; Lions, F. *J. Am. Chem. Soc.* **1962**, 84, 2262-2263. (c) Geldard, J. F.; Lions, F. *Inorg. Chem.* **1963**, 2, 270-282.

(24) Wood, A.; Aris, W.; Brook, D. J. R. *Inorg. Chem.* **2004**, 43, 8355-8360.

Table of Contents

